

DEVELOPMENT OF STRUCTURAL DESIGN PROCEDURES FOR UHPC

Yiming Yao^a, Farrokh Kianmofrad^b, Aashay Arora^c, Narayanan Neithalath^d, Barzin Mobasher^d

a - Associate Professor, Key Laboratory of Concrete and Prestressed Concrete Structures of Ministry of Education, School of Civil Engineering, Southeast University, Nanjing, China

b – Graduate Student, School of Sustainable Engineering and the Built Environment, Arizona State University, Tempe, AZ

c – Post-doctoral Research Scholar, School of Sustainable Engineering and the Built Environment, Arizona State University, Tempe, AZ

d – Professor, School of Sustainable Engineering and the Built Environment, Arizona State University, Tempe, AZ

Abstract

Several procedures for design of UHPC use formulations based on a strain compatibility analysis, which can be extended to a serviceability-based design by incorporation of full material stress-strain relationship. The material models can be implemented in finite element and elastic-plastic solution methodologies in order to close the gap among properties, analysis, modeling, and design. The tensile characteristics of UHPC can be defined in the context of fiber content and response after the matrix has fully cracked. The general terms of strain softening and/or strain hardening are defined, and additional sub-classes of deflection-softening and -hardening may be outlined based on the behavior in bending.

Keywords - UHPC, Hybrid reinforced UHPC, Fiber reinforced UHPC, Serviceability, Design.

1 Introduction

UHPC materials are designed to exhibit noticeable ductility, energy absorption capacity, and post-cracking strength under tension by employing a relatively high dosage of fiber reinforcement (Meda et al., 2012; Yao et al., 2017). The enhanced post-cracking tensile strength and improved crack control due to the distributed fiber reinforcement can improve shear behavior and may potentially substitute or reduce conventional transverse reinforcement (Balaguru et al., 1992; Batson, 1976; Dinh et al., 2010; Lee et al., 2011; Prisco et al., 2009; Soranakom and Mobasher, 2009; Vandewalle, 2002, 1999).

Simplified equations to account for the contribution of fibers to the tensile and shear response, cracking strength, and post-crack softening response are widely used to evaluate the mechanical performance. By representing the bridging force as an average effective tensile stress-crack width relationship (or stress-strain relationship for a specimen of finite width referred to as a localized plastic hinge), one can model the material property as nonlinear spring elements to simulate the residual capacity of a cracked section (Barros et al., 2005; Naaman and Reinhardt, 2006). In many situations, direct interpretation of results primarily based on the strength can be misleading, since the interactions due to variables are not considered. Different cracking mechanisms often lead to conservative interpretations which underestimate the effect of real parameters (Bernard, 2004; Minelli et al., 2007).

2 Parametric Yield Hinge Model

Simulation of the load-deflection response of a flexural member can be used as the basis of analysis and design in many applications. The general closed-form relationship of moment-curvature response can be obtained based on piecewise-linear material constitutive relationships. These formulations can be used in the design of plain, reinforced, as well as fiber reinforced concrete and can also be extended to the calculation of the load-deflection response of UHPC (Soranakom and Mobasher, 2008, 2007). The parametric model can be used to develop a serviceability limit state (SLS) or ultimate limit state (ULS) criteria for the design of FRC flexural members (Soranakom and Mobasher, 2009) using both for strain softening and strain hardening FRC. As an extension to the model, one can also consider a combination of fibers and plain reinforcement in the context of hybrid reinforced concrete (HRC) which addresses structural members that combine continuous reinforcement with randomly distributed chopped fibers in the matrix. (Lim et al., 1987; Lok and Pei, 1998; Taheri et al., 2011; Vandewalle, 2002).

The proposed solution strategy can be used to reduce the total amount of reinforcement, section size, or the ductility of the UHPC mixtures while meeting the ultimate and serviceability flexural stress requirements. In addition, the moment-curvature expressions for homogenized UHPC can be used to analyze the cracking and ductility response as well as estimate the serviceability deflection level.

An analytical model for simulating the flexural behavior of HRC, has been presented by (Mobasher et al., 2015a). Figure 1(a) and (b) present the constitutive model for homogenized strain softening and hardening with two fundamental material parameters: Elastic modulus, E , and first cracking tensile strain, $\varepsilon_{cr} = \sigma_{cr}/E$ and several parametric

variables. The compressive response in Figure 1(a) is elastic-plastic with an initial modulus γE ($\gamma=1$) up to the compressive strength of $\omega \gamma \sigma_{cr}$ where ω represents the ratio of compressive strain capacity to tensile strain cracking, ε_{cr} . The trilinear tension model in Figure 1(b) is defined by an elastic range E , post-cracking modulus $E_{cr}=\eta E$, and residual strength $\sigma_{cst}=\mu \varepsilon_{cr} E=\mu \sigma_{cr}$ in the post-crack region. Three tensile strain measures define the first cracking, transition to constant stress softening, and ultimate strains (ε_{cr} , $\varepsilon_{trn} = \alpha \varepsilon_{cr}$, ε_{tu}). Two non-dimensional strain parameters define the limit-state compressive strain $\varepsilon_{cy} = \omega \varepsilon_{cr}$, and $\varepsilon_{cu} = \lambda_{cu} \varepsilon_{cr}$. The strain variables are also represented as non-dimensional using $\varepsilon_t = \beta \varepsilon_{cr}$, and $\varepsilon_c = \lambda \varepsilon_{cr}$

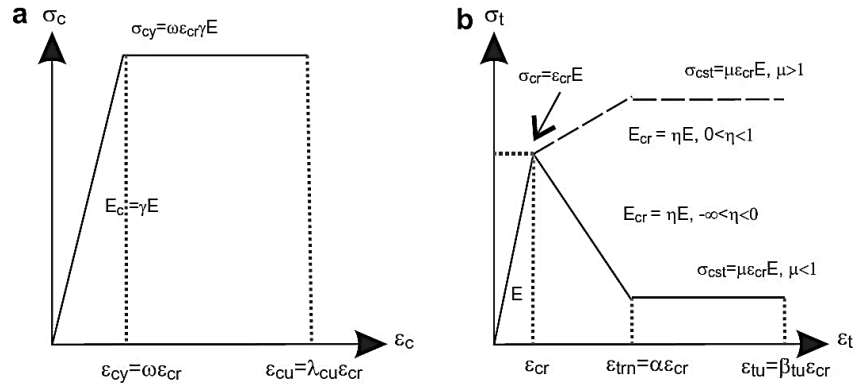


Figure 1. Material models for homogenized fiber reinforced concrete: (a) compression model and (b) tension model (Chote Soranakom and Mobasher, 2007a).

The stress-strain relationship in compression for UHPC is affected by the dense microstructure and fibers, however the tensile capacity does not scale with the increase in compressive strength. The parametric components defined above can be obtained from the experimental closed-loop tension and compression tests or the empirical relations used by various guides and codes. For example, VSL Australia (Gowripalan and Gilbert, 2000) as well as Almansour (Almansour and Lounis, 2010) developed an idealized stress-strain relationship by assuming that the compressive strength is limited to $0.85f'_c$ (i.e., $\beta_2=0.85$), and tensile strength is 4% of the compressive strength, the normalized compressive strength ω is then obtained as Eq 1, with similar approaches adopted for ACI 318, or Model code.

$$\omega = \frac{\varepsilon_{cy}}{\varepsilon_{cr}} \approx \frac{\beta_2 f'_c}{\sigma_{cr}} = \frac{0.85 f'_c}{0.04 f'_c} \approx 20 \quad (1)$$

The flexural response is measured using the closed-form solutions of moment-curvature response through a sectional analysis (Mobasher et al., 2015a). The detailed derivations for strain softening, strain hardening FRC as well as hybrid reinforced concrete (HRC) section containing both rebar and fibers can be found in (Mobasher et al., 2015b; Chote Soranakom and Mobasher, 2007b; C. Soranakom and Mobasher, 2007; Soranakom and Mobasher, 2008b) and summarized in Table 1. These equations address the interactions

among different stages in tension and compression models, where the parameterized functions are all normalized with respect to the cracked section modulus, and:

$$M = M' M_{cr} \quad , M_{cr} = \frac{\sigma_{cr} b h^2}{6} \quad , \quad \varphi = \varphi' \phi_{cr} \quad , \quad \phi_{cr} = \frac{\varepsilon_{cr}}{2h} \quad , \quad \phi'_i = \frac{\beta}{2(1-k_i)} \quad (1)$$

Table 1 Normalized Neutral axis depth k , normalized moment M_i' and curvature ϕ' for each stage i of normalized tensile strain at bottom fiber (β)

Stage	k	M_i'
1 $0 < \beta \leq 1$	$k_1 = \begin{cases} \frac{1}{2} & \text{for } \gamma=1 \\ \frac{-1+\sqrt{\gamma}}{-1+\gamma} & \text{for } \gamma < 1 \text{ or } \gamma > 1 \end{cases}$	$M'_1 = \frac{2\beta[(\gamma-1)k_1^3 + 3k_1^2 - 3k_1 + 1]}{1-k_1}$
2.1 $1 < \beta \leq \alpha$ $0 < \lambda \leq \omega$	$k_{21} = \frac{\beta^2\gamma + D_{21} - \sqrt{\gamma^2\beta^4 + D_{21}\gamma\beta^2}}{D_{21}}$ $D_{21} = \eta(\beta^2 - 2\beta + 1) + 2\beta - \beta^2\gamma - 1$	$M'_{21} = \frac{(2\beta\gamma + C_{21})k_{21}^3 - 3C_{21}k_{21}^2 + 3C_{21}k_{21} - C_{21}}{1-k_{21}}$ $C_{21} = (-2\eta\beta^3 + 3\eta\beta^2 - 3\beta^2 - \eta + 1)\beta^{-2}$
2.2 $1 < \beta \leq \alpha$ $\omega < \lambda \leq \lambda_{cu}$	$k_{22} = \frac{D_{22}}{D_{22} + 2\omega\gamma\beta}$ $D_{22} = \eta(\beta^2 - 2\beta + 1) + 2\beta + \omega^2\gamma - 1$	$M'_{22} = (3\omega\gamma + C_{22})k_{22}^2 - 2C_{22}k_{22} + C_{22}$ $C_{22} = (2\eta\beta^3 - 3\eta\beta^2 + 3\beta^2 - \omega^3\gamma + \eta - 1)\beta^{-2}$
3.1 $\alpha < \beta \leq \beta_{tu}$ $0 < \lambda \leq \omega$	$k_{31} = \frac{D_{31} - \sqrt{\gamma\beta^2 D_{31}}}{D_{31} - \beta^2\gamma}$ $D_{31} = \eta(\alpha^2 - 2\alpha + 1) + 2\mu(\beta - \alpha) + 2\alpha - 1$	$M'_{31} = \frac{(C_{31} - 2\beta\gamma)k_{31}^3 - 3C_{31}k_{31}^2 + 3C_{31}k_{31} - C_{31}}{k_{31} - 1}$ $C_{31} = (3(\mu\beta^2 - \mu\alpha^2 - \eta\alpha^2 + \alpha^2) + 2\eta\alpha^3 + \eta - 1)\beta^{-2}$
3.2 $\alpha < \beta \leq \beta_{tu}$ $\omega < \lambda \leq \lambda_{cu}$	$k_{32} = \frac{D_{32}}{D_{32} + 2\omega\gamma\beta}$ $D_{32} = \omega^2\gamma + \eta\alpha^2 + 2(\mu\beta - \eta\alpha - \mu\alpha + \alpha) + \eta - 1$	$M'_{32} = (C_{32} + 3\omega\gamma)k_{32}^2 - 2C_{32}k_{32} + C_{32}$ $C_{32} = \frac{3(\mu\beta^2 - \mu\alpha^2 - \eta\alpha^2 + \alpha^2) + 2\eta\alpha^3 - \omega^3\gamma + \eta - 1}{\beta^2}$

2.1 Ultimate Strength and Ultimate Limit State for Plain UHPC Beams in Flexure

The flexural capacity of a UHPC section can be viewed in terms of three strength parameters, the first one represents the first cracking of the section under a linear elastic response, the second is the equivalent strength obtained at the maximum load carried by the section and this is normally obtained at a point where the tensile crack has progressed along the section depth. This maximum load obtained under a flexural loading is converted to an elastic equivalent ultimate strength.

For the serviceability based design criteria, the maximum load can be obtained analytically by the interaction of various modes of loading. The third and final strength parameter is the limit state which is obtained as the stress at the cracked section stabilizes at the residual tensile strength of the material. In this case the fiber phase is resisting the load and the strain or deflection is increased up to a limiting crack width. The capacity at this stage can be obtained using asymptotic analysis and presented in terms of the parametric variables represented in Equation 2 as discussed in (Arora et al., 2019)

$$M_n = \frac{\omega\mu(3\omega + 8\mu)}{(\omega + 2\mu)^2} M_{cr} \quad M_{cr} = \frac{\sigma_{cr}bh^2}{6} \quad (2)$$

Using a value of $\omega=20$ in Equation 2, the nominal moment capacity at limit state can be expressed within 0.5% accuracy as $M_n = 2.85\mu M_{cr}$ which is similar to the analytical limit for the ultimate design capacity obtained as $M_n = 3\mu M_{cr}$ by (Soranakom and Mobasher, 2008a) for a bilinear elastic-residual strength material and in line with the experimental predictions of $M_n = 2.85\mu M_{cr}$ (Bakhshi et al., 2014; Graybeal, 2014). Using the moment-curvature closed form equations, it is possible to simulate the load-deflection response of a beam using the moment-area method or other closed form approaches as well (Yao et al., 2017).

2.2 Ultimate Limit State for Hybrid Reinforced Concrete (HRC)

The HRC analytical model presented by (Mobasher et al., 2015a) is used in a design approach applied to the UHPFRC members. Equations to determine the moment-curvature relationship, ultimate moment capacity, and minimum flexural reinforcement ratio were explicitly derived (Mobasher, 2011). The arrangement of the rebars within a cross-section of width b and depth h is used to obtain the centroid of the reinforcement at a distance $d=\alpha h$. Several other parameters are defined to consider the elastic modulus, yield strain in steel, $E_s=nE_c$, $\varepsilon_{sy}=\kappa\varepsilon_{cr}$ and reinforcement ratio, $A_s=\rho_gbh$ respectively. The closed form equations for these cases have also been developed which may be easily replaced with the moment curvature relationship represented in the Table 1. Regardless of the reinforcement type and content, the net effect on the cross-sectional analysis is the updated moment-curvature relationship.

3 Design Tools For Serviceability Based Limit State (SLS)

A sustainability-based approach enables the designer to follow different deformation stages in tension and compression layers and predict the response of the section under a specific service level of imposed tensile strain, ε_t (or parameter β). This approach allows one to specify the desired deflection (curvature) of the section and then to calculate the equivalent tensile strain at the bottom fiber and the relevant moment capacity (Chote Soranakom and Mobasher, 2007a; Soranakom and Mobasher, 2008a, 2009; Mobasher et al., 2015a).

The equations of Table 1 can be further simplified using polynomial or power curve fitting with detailed application for individual cases presented in (Mobasher, 2011) as demonstrated by an example of design procedure. The first step is the representation of moment curvature for a series of set values of various parameters. For example, calculation of the neutral axis under the two cases of tension cracking (range 2.1) and tension softening (3.1) where compression response is assumed to be elastic is defined as a function of strain parameter $\beta = \varepsilon_t / \varepsilon_{cr} < \beta_{tu}$ is obtained as:

$$k_{21} = \frac{\sqrt{A_{21}}}{\sqrt{A_{21} + \beta\sqrt{\gamma}}} \quad A_{21} = \eta(\beta^2 + 1 - 2\beta) + 2\beta - 1$$

$$k_{31} = \frac{\sqrt{A_{31}}}{\sqrt{A_{31} + \beta\sqrt{\gamma}}} \quad A_{31} = \eta(\alpha^2 + 1 - 2\alpha) + 2\mu(\beta - \alpha) + 2\alpha - 1$$
(7)

In order to simplify the process, one can use a curve fitting algorithm to generate the moment capacity and moment-curvature response for any cross section using basic tensile material parameters and represent the results using curve-fit parameters. For example, for a given material with specific tensile stress strain response, one can obtain the parameters and generate the master moment-curvature-neutral axis curves. Figure 2 and Table 2 show the case of ($\eta=0.0001-0.5$, $\gamma=1$ and $\alpha=51$), and for different values of post-crack stiffness, $\mu=1.0, 0.67, 0.33, 0.0$ where β_{tu} is assumed to be equal to 200. The moment-curvature-neutral axis relationships are now developed as a function of applied strain or the curvature for that specific material and can be represented as a function of remaining parameters.

Results of Figure 2 show that an increase in applied tensile strain leads to a decrease in the neutral axis compression zone depth. The transitional black line represents the elastic perfectly-plastic response of the section, ($\eta=0.0$). Blue lines belong to the strain-softening ($\eta < 0$) response and the red curves stand for the strain-hardening ($\eta > 0$) behavior.

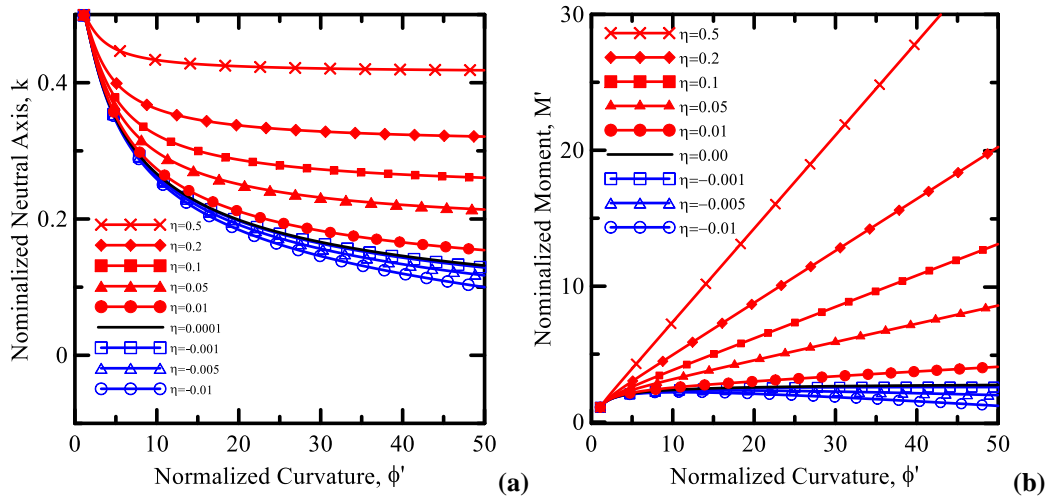


Figure 2. Effect of a) Depth of Neutral axis on the Moment capacity of a section for strain softening and hardening and b) the moment-curvature response in the Range 2.1

The neutral axis k is a function of applied strain β and is used to obtain the moment-curvature relationship. Figure 3 demonstrates a 3D plot of moment and curvature diagram for a specific limiting strain such as $\beta = \beta_{tu} = 50$. These plots can be achieved for other β values. Figure 4 illustrates the superimposed results from each range (i.e., ranges 1, 2-1, and 3-1) and the final simulated moment-curvature diagram. This figure shows that as the curvature (and therefore the strain in the lower fiber of the section, β) increases, the calculated moment moves from one range to others. For the HRC sections the occurrence of the compressive failure is also possible.

Table 2. Location of the neutral axis, moment, and curvature of a composite material with $\gamma = 1$ and $\eta = 0.0001- 0.5$, and 3.1 range $\gamma = 1$, $\alpha = 51$ and $\mu = 0.00- 1.00$.

Range	η, μ	$A, (k = \frac{\sqrt{A}}{\sqrt{A} + \beta})$	$M'(k)$	$M'(\varphi)$
2.1	$\eta=0.5$	$0.5(\beta^2 + 1 - 2\beta) + 2\beta - 1$	$1.36 + 2.3 \times 10^{-8} \exp(k^{-3.5})$	$0.503 + 0.686\varphi$
2.1	$\eta=0.2$	$0.2(\beta^2 + 1 - 2\beta) + 2\beta - 1$	$1.538 + 0.00115 \exp(k^{-2})$	$1.097 + 0.383\varphi$
2.1	$\eta=0.1$	$0.1(\beta^2 + 1 - 2\beta) + 2\beta - 1$	$2.124 + 0.00595 \exp(k^{-1.5})$	$1.459 + 0.233\varphi$
2.1	$\eta=0.05$	$0.05(\beta^2 + 1 - 2\beta) + 2\beta - 1$	$1.001 + 0.06872 \exp(k^{-1})$	$1.73 + 0.1376\varphi$
2.1	$\eta=0.01$	$0.01(\beta^2 + 1 - 2\beta) + 2\beta - 1$	$0.7293 + 0.2582 \exp(k^{-0.5})$	$1.208 + 0.4004\sqrt{\varphi}$
2.1	$1e-4$	$0.0001(\beta^2 + 1 - 2\beta) + 2\beta - 1$	$6.42 - 3.527 \exp(k^{1.5})$	$3.014 - 2.028 / \sqrt{\varphi}$
3.1	$\eta = -1e-3$	$-(\beta^2 + 1 - 2\beta) \times 10^{-3} + 2\beta - 1$	$9.669 - 7.043 \exp(k^{2.5})$	$2.649 - 2.201 / \varphi$
3.1	$\mu = 1.$	$2\beta - 1$	$5.041 - 2.038 \exp(k)$	$-4.74 + 1.75 \exp(\varphi^{-0.5})$
3.1	$\mu = 0.67$	$1.34\beta + 16.16$	$-2347 + 2349 \exp(k^5)$	$-5362 + 5364 \exp(\varphi^{-3})$
3.1	$\mu = 0.33$	$0.66\beta + 33.84$	$-227.9 + 228.9 \exp(k^3)$	$-519.7 + 521 \exp(\varphi^{-2})$
3.1	$\mu = 0.00$	51	$-65.86 + 65.86 \exp(k^2)$	$-845 + 845 \exp(\varphi^{-2})$

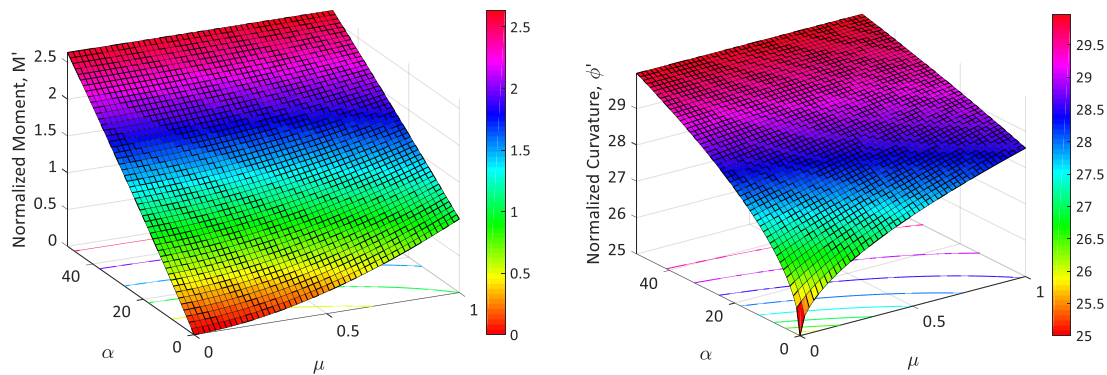


Figure 3. 3D plot of moment and curvature diagrams ($\lambda=1$, $\omega=30$, and $\beta=\beta_{tu}=50$).

Figure 5 illustrates the effect of parameters μ and β representing the residual tensile strength and the applied tensile strain on the moment-curvature response. The parametric studies are expressed in terms of tensile strain, β , for different levels of post-crack tensile strength (residual strength) parameter, μ from brittle ($\mu=0$) to ductile response ($\mu=1.0$). From these curves, the value for the moment and curvature can be obtained at any specific tensile strain, for any section.

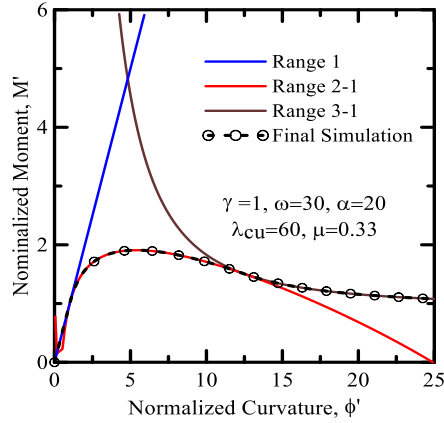


Figure 4. Superimposed responses of each range and the final simulated moment-curvature diagram.

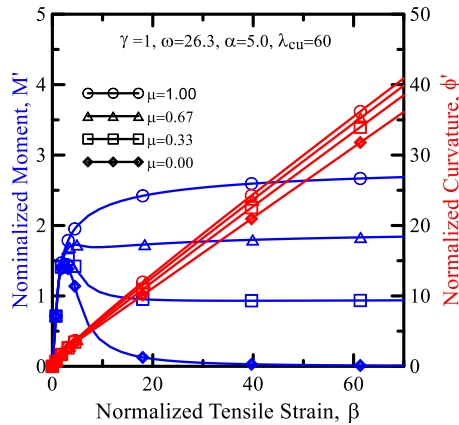


Figure 5. Normalized moment-curvature diagram as a function of tensile strain, β , for different levels of post-crack tensile strength (residual strength) parameter, μ .

4 Comparison with Experimental data

Kaka and Chao (Kaka and Chao, 2018) compared prestressed concrete structures with UHPC structural members. Results of two simply supported beams, made of UHPC and monotonically loaded to failure are shown in Figure 6. The beam specimen dimensions were a width of 9" (229 mm), height of 16" (406 mm), and a span length of 134" (3404 mm). A 20" (508 mm) constant moment region was at the mid-span of all specimens. The shear span to effective-depth ratio, a/d was 3.93 and ASTM A1035 high-strength corrosion-resistant low-carbon chromium reinforcing bars for both specimens. No shear

reinforcement was used. The comparison graphs between the experimental results and the simulated results, using the constitutive analytical model are presented in Figure 6b and show a good agreement. The effective tensile stress strain response necessary to simulate the model is also shown. The analytical model can be used up to any specified allowable strain or curvature level, therefore this approach allows one to design such reinforced concrete members without total reliance on the limit state design and the computations can be applied for ant prescribed strain level.

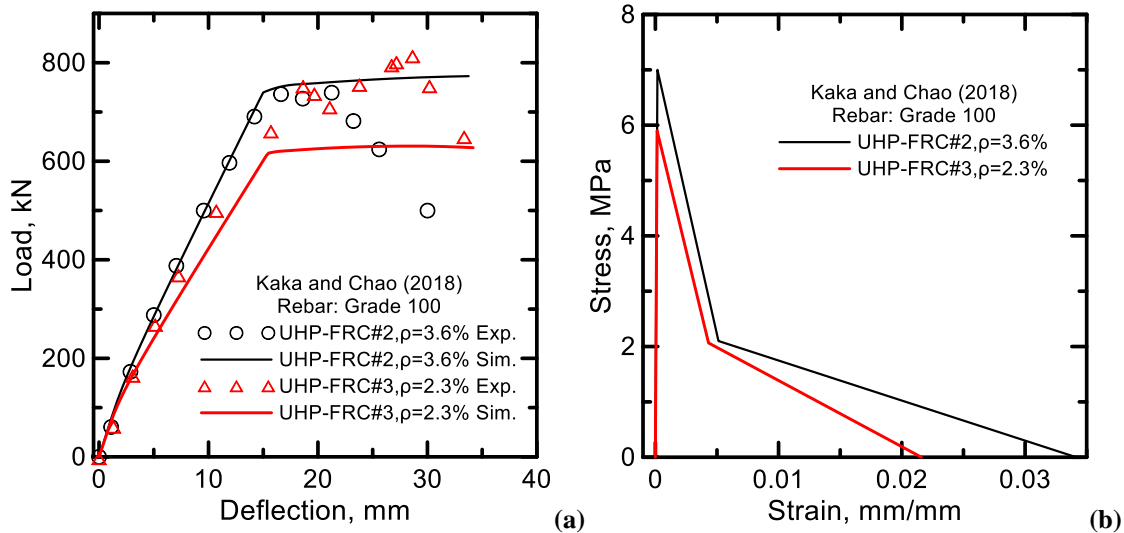


Figure 6. a) Simulated load-deflection curves; b) Stress-strain graphs for tensile behavior.

5 Conclusions

Analytical approaches to evaluate the flexural capacity of the FRC, HRC and UHPC sections have been developed using a general approach to define the moment-curvature relationship of a section using material properties that are represented as piecewise linear models. The equations for general cross-sectional analysis are obtained. This approach can be used for the serviceability and ultimate limit state designs. The closed form solutions can be converted to accurate curve fit relationships for various material types. The proposed approaches were investigated using the experimental results from available UHPC reinforced section beam testing results.

6 Acknowledgements

The authors sincerely acknowledge the Arizona Department of Transportation (ADOT) for funding this research (Grant no: SPR 745). The materials used were provided by BASF Corporation, Salt River Materials Group, Holcim Cement, Burgess Pigments, and Omya A.G., and their contributions are acknowledged. The contents of this paper reflect the views of the authors who are responsible for the facts and accuracy of the data presented herein, and do not necessarily reflect the views and policies of the funding agency, nor do the contents constitute a standard, specification, or a regulation.

7 References

- Almansour, H., Lounis, Z., 2010. Innovative design approach of precast–prestressed girder bridges using ultra high performance concrete. *Can. J. Civ. Eng.* 37, 511–521.
- Arora, A., Yao, Y., Aguayo, M., Kianmofrad, F., Neithalath, N., Mobasher, B., 2019. SPR 745–Developing Ultra-High-Performance Concrete Mix Designs for Arizona Bridge Element Connections (Under Review by ADOT).
- Bakhshi, M., Barsby, C., Mobasher, B., 2014. Comparative evaluation of early age toughness parameters in fiber reinforced concrete. *Mater. Struct.* 47, 853–872. <https://doi.org/10.1617/s11527-013-0098-1>
- Balaguru, P., Narahari, R., Patel, M., 1992. Flexural toughness of steel fiber reinforced concrete. *Mater. J.* 89, 541–546.
- Barros, J.A.O., Cunha, V.M.C.F., Ribeiro, A.F., Antunes, J. a. B., 2005. Post-cracking behaviour of steel fibre reinforced concrete. *Mater. Struct.* 38, 47–56. <https://doi.org/10.1007/BF02480574>
- Batson, G., 1976. Steel fiber reinforced concrete. *Mater. Sci. Eng.* 25, 53–58.
- Bernard, E.S., 2004. Durability of cracked fibre reinforced shotcrete. *Shotcrete More Eng. Dev.* Taylor Francis Lond. ES Bernard Ed 59–66.
- Destrée, X., Yao, Y., Mobasher, B., 2015. Sequential Cracking and Their Openings in Steel-Fiber-Reinforced Joint-Free Concrete Slabs. *J. Mater. Civ. Eng.* 28. [https://doi.org/10.1061/\(ASCE\)MT.1943-5533.0001377](https://doi.org/10.1061/(ASCE)MT.1943-5533.0001377)
- Dinh, H.H., Parra-Montesinos, G.J., Wight, J.K., 2010. Shear strength model for steel fiber reinforced concrete beams without stirrup reinforcement. *J. Struct. Eng.* 137, 1039–1051.
- Gowripalan, N., Gilbert, R.I., 2000. Design guidelines for RPC prestressed concrete beams. *Syd. Aust. Sch. Civ. Environ. Eng. Univ. New South Wales.*
- Graybeal, B., 2014. Design and construction of field-cast UHPC connections.
- Kaka, V.B., Chao, S.-H., 2018. Investigation of Eliminating Prestress in Bridge Girders with the Use of Non-Prestressed Ultra-High-Performance Fiber-Reinforced Concrete Girders, in: *Structures Congress 2018*. American Society of Civil Engineers Reston, VA, pp. 65–80.
- Lee, S.-C., Cho, J.-Y., Vecchio, F.J., 2011. Diverse embedment model for steel fiber-reinforced concrete in tension: model development. *Mater. J.* 108, 516–525.
- Lim, T.Y., Paramisivam, P., Lee, S.L., 1987. Bending behavior of steel-fiber concrete beams. *Struct. J.* 84, 524–536.
- Lok, T.-S., Pei, J.-S., 1998. Flexural behavior of steel fiber reinforced concrete. *J. Mater. Civ. Eng.* 10, 86–97.
- Meda, A., Minelli, F., Plizzari, G.A., 2012. Flexural behaviour of RC beams in fibre reinforced concrete. *Compos. Part B Eng.* 43, 2930–2937.
- Minelli, F., Plizzari, G.A., Vecchio, F.J., 2007. Influence of steel fibers on full-scale RC beams under shear loading, in: *High Performance Concrete, Brick-Masonry and Environmental Aspects. Sixth International Conference of Fracture Mechanics of Concrete and Concrete Structures FRAMCOS6*. Taylor & Francis Group (UK), London/Catania. pp. 1523–1531.

- Mobasher, B., 2011. Mechanics of fiber and textile reinforced cement composites. CRC press.
- Mobasher, B., Yao, Y., Soranakom, C., 2015a. Analytical solutions for flexural design of hybrid steel fiber reinforced concrete beams. *Eng. Struct.* 100, 164–177.
- Mobasher, B., Yao, Y., Soranakom, C., 2015b. Analytical solutions for flexural design of hybrid steel fiber reinforced concrete beams. *Eng. Struct.* 100, 164–177. <https://doi.org/10.1016/j.engstruct.2015.06.006>
- Naaman, A.E., Reinhardt, H.W., 2006. Proposed classification of HPFRC composites based on their tensile response. *Mater. Struct.* 39, 547–555. <https://doi.org/10.1617/s11527-006-9103-2>
- Prisco, M. di, Plizzari, G., Vandewalle, L., 2009. Fibre reinforced concrete: new design perspectives. *Mater. Struct.* 42, 1261–1281. <https://doi.org/10.1617/s11527-009-9529-4>
- Soranakom, C., Mobasher, B., 2009. Flexural Design of Fiber-Reinforced Concrete. *Mater. J.* 106, 461–469. <https://doi.org/10.14359/51663147>
- Soranakom, C., Mobasher, B., 2008a. Correlation of tensile and flexural responses of strain softening and strain hardening cement composites. *Cem. Concr. Compos.* 30, 465–477.
- Soranakom, C., Mobasher, B., 2008b. Correlation of tensile and flexural responses of strain softening and strain hardening cement composites. *Cem. Concr. Compos.* 30, 465–477. <https://doi.org/10.1016/j.cemconcomp.2008.01.007>
- Soranakom, Chote, Mobasher, B., 2007a. Closed-form solutions for flexural response of fiber-reinforced concrete beams. *J. Eng. Mech.* 133, 933–941.
- Soranakom, Chote, Mobasher, B., 2007b. Closed-Form Moment-Curvature Expressions for Homogenized Fiber-Reinforced Concrete. *Mater. J.* 104, 351–359.
- Soranakom, C., Mobasher, B., 2007. Closed-Form Solutions for Flexural Response of Fiber-Reinforced Concrete Beams. *J. Eng. Mech.* 133, 933–941. [https://doi.org/10.1061/\(ASCE\)0733-9399\(2007\)133:8\(933\)](https://doi.org/10.1061/(ASCE)0733-9399(2007)133:8(933))
- Taheri, M., Barros, J.A.O., Salehian, H., 2011. A design model for strain-softening and strain-hardening fiber reinforced elements reinforced longitudinally with steel and FRP bars. *Compos. Part B Eng.* 42, 1630–1640. <https://doi.org/10.1016/j.compositesb.2011.04.009>
- Vandewalle, L., 2002. RILEM TC162-TDF : Test and Design methods for Steel Fibre Reinforced Concrete : Bending test (final recommendation). *Mater. Struct.* 35, 579–582.
- Vandewalle, L., 1999. Influence of Tensile Strength of Steel Fibre on the Toughness of High Strength Concrete, in: Third International Workshop " High Performance Fiber Reinforced Cement Composites". pp. 331–340.
- Yao, Y., Wang, X., Aswani, K., Mobasher, B., 2017. Analytical procedures for design of strain softening and hardening cement composites. *Int. J. Adv. Eng. Sci. Appl. Math.* 9, 181–194.